COMSOL CONFERENCE 2025 AMSTERDAM

Towards high thermal-to-hydraulic performance of heat exchangers for water-gravel thermal energy storage

A. Dahash[1], F. Giordano[1], A. Serageldin[1], Emre Bas[2], Rainer Strobel[2]
1. Center for Energy, AIT Austrian Institute of Technology GmbH, Vienna, Austria.
2. Planungsgruppe M+M AG, Böblingen, Germany.

Abstract
Water-gravel thermal energy storage (WGTES) offers a cost-effective and environmentally sustainable solution for large-scale seasonal thermal energy storage, with performance strongly dependent on the layout and operation of charging and discharging heat exchangers. This study presents a simulation-driven methodology for optimizing heat exchanger design in a WGTES with three neighboring storage units at the incampus demo site of the INTERSTORES project.
A detailed COMSOL Multiphysics® model is developed to capture both thermal and hydraulic interactions between the heat exchangers and the porous gravel matrix. Parametric analyses investigate different heat exchanger configurations. Performance is assessed via a thermal-to-hydraulic ratio. Results show that layout, multi-level configurations and operating conditions significantly affect thermal performance, hydraulic losses and overall efficiency.
This work demonstrates the value of multiphysics modeling for performance-optimized WGTES design and provides a transferable framework for large-scale seasonal storage planning.
Keywords: Water-gravel thermal energy storage; seasonal thermal energy storage; indirect charging and discharging; heat exchangers; pipe flow module; incampus.

Introduction
Seasonal thermal energy storage (sTES) arises as a key technology that will play a pivotal role in the future of district heating (DH) systems, particularly as renewable energy sources (RES) such as solar energy become increasingly integrated [1]. Given the seasonal mismatch between renewable energy supply and heating demand, these storage systems typically require large storage volumes [2]. When integrated into renewable-based district heating (R-DH), sTES technologies provide the flexibility needed to balance temporal fluctuations in energy generation and consumption [1]. Moreover, DH systems can also utilize non-seasonal renewable or residual heat sources, including geothermal energy and industrial or municipal waste heat [3].
Because sTES systems are generally buried underground (partially or fully) or located near the surface, they are often categorized as underground thermal energy storage (UTES) systems. Among the main UTES concepts described in the literature, the most commonly implemented are: (1) aquifer thermal energy storage (ATES), (2) borehole thermal energy storage (BTES), (3) tank thermal energy storage (TTES), (4) pit thermal energy storage (PTES) and (5) cavern thermal energy storage (CTES). The selection of a suitable technology depends largely on local hydrogeological conditions and target temperature levels. ATES and BTES are typically applied in low-temperature DH networks, whereas PTES, CTES and TTES are preferred for high-temperature applications (60°C-140°C).
Despite their clear potential, large-scale sTES systems still face significant deployment challenges, including high investment costs, large spatial footprints, and complex design and permitting procedures.
Most of the implemented sTES systems worldwide rely on sensible, water-based storage due to water high specific heat capacity (4.18 MJ/(m³·K) between 10°C and 95°C) [2]. This property enables high indirect charging and discharging rates and makes water an efficient and widely accessible storage medium. However, the use of water introduces structural and mechanical challenges, particularly concerning the design and stability of the cover structure, which must withstand both hydrostatic and thermal stresses.
An alternative approach employs solid storage media, offering improved mechanical stability and the potential for simpler and more cost-effective structural designs. This can reduce overall investment costs and facilitate wider market adoption. One such configuration is the water-gravel thermal energy storage (WGTES) system, in which gravel serves as the primary storage medium. The inclusion of solid material decreases the structural demands on the tank or pit, thus lowering construction complexity and costs.

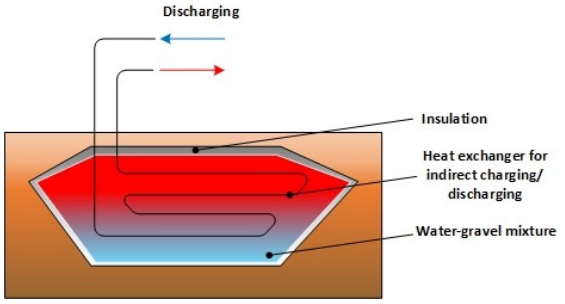

Figure 1: Indirect discharge through an embedded heat exchanger within water-gravel PTES.

Because WGTES systems typically rely on indirect heat transfer through embedded heat exchangers, the optimal design and control of charging and discharging cycles are critical to achieve high system efficiency and acceptable thermal response times. Therefore, this work will optimize the design and layout of charging/discharging heat exchangers for a real-life WGTES application.

Methodology

Case Study: incampus

The incampus is a 75-hectare industrial estate located in Ingolstadt (DE) on the former site of a decommissioned refinery near the Danube River. The area is being jointly redeveloped by AUDI AG and the City of Ingolstadt into an innovative business park and technology center. The transformation of the site follows a comprehensive sustainability strategy emphasizing resource efficiency and circular use of existing infrastructure [4].

A notable feature of this redevelopment is the repurposing of the legacy infrastructure – namely former firefighting water basins – into sTES system. In the envisioned local energy system, these sTES units will enhance flexibility and enable greater integration of RESs. To minimize the primary energy demand, the overall heating and cooling concept is designed to exploit locally available low-temperature energy sources and sinks, including groundwater, river water, geothermal energy and industrial waste heat. Further details on the system can be found in [4].

The focus of this work lies mainly on the sTES system within the incampus energy concept as this will be a water-gravel thermal energy storage (WGTES) system with a net volume of approx. 18,000 m³ as shown in Figure 2. Therein, the basic C is the core of this study, which has a total volume of approx. 5280 m^3. The storage medium is a mixture of water-gravel with a porosity of 0.4, the equivalent density of the water-gravel mixture is 1,420 kg/m³ [5], and the specific heat capacity is 1,800 J/(kg·K), yielding a volumetric heat capacity of 2,556 kJ/(m³·K).

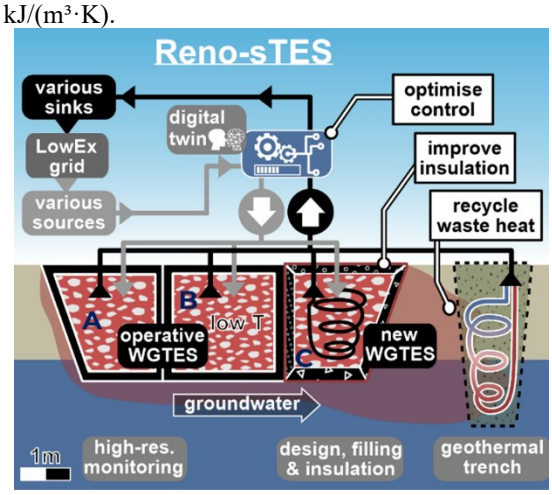

Figure 2: WGTES system at incampus site.

DePlaTES Framework

In COMSOL Multiphysics®, a comprehensive detailed planning toolkit for sTES systems known as "*DePlaTES*" is developed. The structure and workflow of *DePlaTES* are illustrated in Figure 3 and further described in [6] and [7].

The *DePlaTES* toolkit comprises two principal components: one representing the sTES system itself and another describing the subsurface environment hosting the storage. DePlaTES offers extensive flexibility in configuring sTES designs, including construction type (partially or fully buried), geometry (tank, pit, or cavern), storage medium (e.g., water, gravel), number and arrangement of charging/discharging ports and insulation materials. Moreover, the subsurface module allows users to define groundwater presence and flow conditions, heterogeneous soil layers, and other geotechnical parameters. The user can specify the intended location of the sTES installation, prompting the toolkit to automatically import reference meteorological data for that site. Alternatively, measured local data can be imported if available.

The *DePlaTES* framework has been validated and benchmarked in several studies to obtain trust and confidence in its predictive capability. Further details on the model development, structure and validation can be found in [6] and [7].

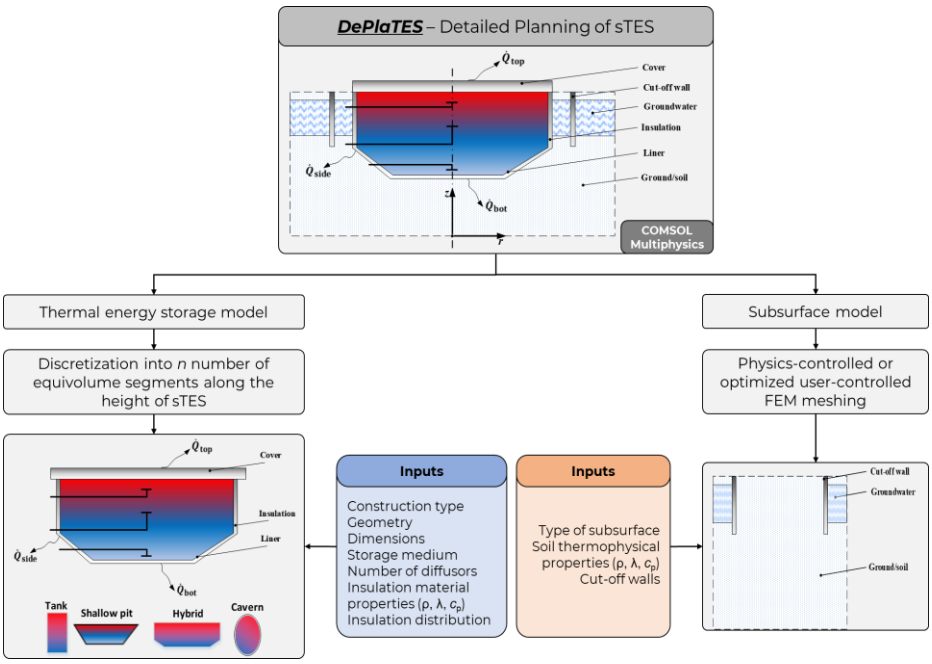

Figure 3: Structure of DePlaTES as implemented in COMSOL Multiphysics®. DePlaTES encompasses two sub models one considers large-scale TES (left-hand side) and the other focuses on the subsurface (right-hand side) [6].

Designs for Charging and Discharging Heat Exchangers

For indirect charging and discharging, the Tichelmann concept (also known as the reverse return flow configuration) is a well-established hydraulic design used in heating and cooling systems to ensure uniform fluid flow distribution across multiple parallel branches [8]. When applied to sTES systems, this principle provides a robust approach for achieving consistent heat transfer and efficient operation. Figure 4 illustrates the double-sided Tichelmann configuration (H1) during charging.

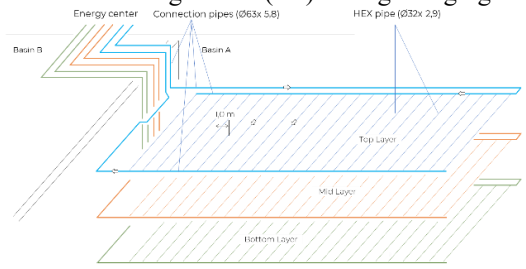

Figure 4: Double-sided Tichelmann concept (H1) for indirect heat transfer showcasing charging conditions.

In this layout (H1), the supply and return headers are arranged such that each flow path has an equal combined length. As a result, all parallel branches experience the same pressure drop, ensuring uniform flow distribution across the system. This uniformity minimizes temperature imbalances, prevents uneven charging or discharging, and reduces the risk of local overheating or incomplete stratification. The main advantages of the double-sided Tichelmann configuration include (i) balanced thermal distribution, (ii) enhanced operational stability, and (iii) lower pumping energy requirements due to optimized hydraulic resistance. However, it also introduces installation complexity and higher capital costs resulting from precise pipe routing and balancing requirements. Moreover, the system's vulnerability to pipe damage means that a failure in a single line could interrupt the operation of the entire layer.

To address this drawback, a second novel configuration (H2) is proposed in Figure 5. Here, each heat-exchange level contains multiple extended loops such that the flow in each loop is independent from the other. Therefore, if one loop fails, the heat exchange level can still be used since the other loops can experience a flow. However, this configuration might lead to higher longitudinal pressure losses and inhomogeneous flow pattern, while on the other hand, the U-Shape of the tube reduces local losses at the flow inversion region.

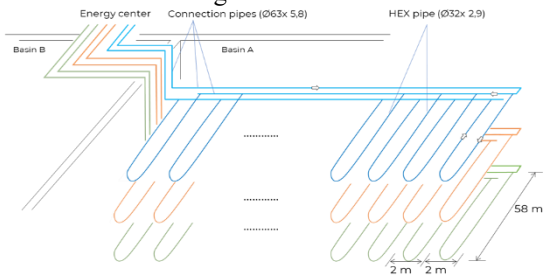

Figure 5: Single-sided Tichelmann concept (H2) for indirect heat transfer showcasing charging conditions

Another modified loop configuration is developed as shown in Figure 6 and known as single-sided Tichelmann concept (H3). It divides each heat-transfer level into multiple independent loops, maintaining the hydraulic balance of the Tichelmann layout while allowing continued operation in case of localized damage. If one loop fails, it can be separated, and the remaining loops remain functional. Although this design enhances resilience, the closer proximity of supply and return pipes increases heat dissipation, slightly reducing heat-transfer effectiveness. Due to the constant flowrate in each heat exchange level, the heat transfer fluid (HTF) experiences the same velocity in all loops leading to uneven heat exchange with the storage medium as the longer paths result in bigger heat exchange area, whereas the shortest one smaller area. Furthermore, this geometry may introduce higher pressure losses due to longer flow paths.

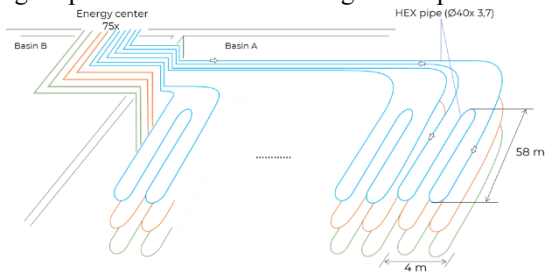

Figure 6: Single-sided Tichelmann concept (H3) for indirect heat transfer showcasing charging conditions.

Figure 7 illustrates the geometric arrangement and spacing of the heat exchanger levels within the storage basin C. The system comprises three horizontal heat exchanger layers (top, middle and bottom) positioned to ensure uniform thermal coverage across the storage domain. The vertical spacing between the top/bottom and mid-level is 0.88 m, while the distance between the top/bottom and upper/bottom storage edge is 0.44 m. Each level consists of evenly distributed parallel loops embedded within the storage medium.

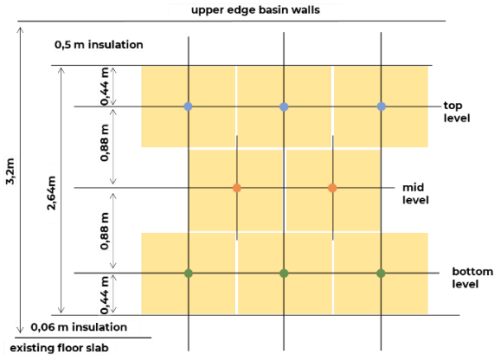

Figure 7: Schematic representation of the geometric configuration for the heat exchanger levels within the storage basin C in the incampus.

Thermal insulation of 0.5 m on the top boundary and 0.06 m at the base will minimize thermal losses to the surroundings, while the existing floor slab of the former basin serves as the structural foundation. The overall basin height is 3.2 m, whereas the effective storage height is 2.64 m.

Simulation Setup

Figure 8 illustrates the geometry representation of basin C at incampus site. The key design parameters and boundary conditions in the simulations are summarized in Table 1. The heat transfer fluid (HTF) used during charging/discharging of WGTES is water and its thermophysical properties used for the simulations are reported in Table 2.

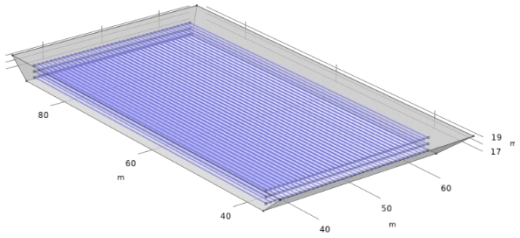

Figure 8: WGTES system geometry – Basin C.

Table 1: *Key design parameters for basin C at incampus.*

Parameter	Value
Top element length	58 m
Top element width	30.5 m
Bottom element length	50.1 m
Bottom element width	26.9 m
Basin Right-side slope	33.8°
Basin left-side slope	88°
Basin C total volume	5280 m^3
Basin C net volume	4165 m^3

Table 2: *Thermophysical properties used in the simulations.*

Parameter	Value
Water thermal conductivity	$k = f(\mathrm{T})$
Water specific heat capacity	$c_p = f(\mathrm{T})$
Water density	$\rho = f(\mathrm{T})$
Convective heat transfer coefficient	$h_{int} = f(\mathrm{Nu})$

The simulation setup is shown in Figure 9 and it couples *Heat transfer in porous media* with *Porous media flow* to capture convection and buoyancy-driven effects within basin C of incampus system, while *Nonisothermal pipe flow* captures the charging and discharging of the basin considered. Additionally, *Moist porous media* module is planned for integration in *DePlaTES* to evaluate moisture penetration and accumulation in bulk insulation materials within storage envelopes.

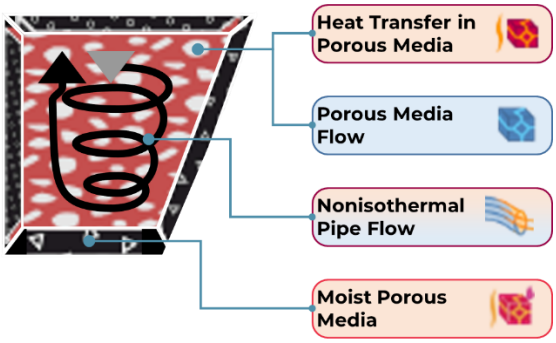

Figure 9: An illustrative sketch for a single basin (Basin C) showing model setup and used/planned modules for the simulation of incampus WGTES.

Since the *Nonisothermal pipe flow* module is employed and water is the heat transfer fluid (HTF), the internal convective heat transfer coefficient h_{int} is computed from the local Nusselt number as follows:

$$h_{\text{int}} = \text{Nu} \cdot \frac{k}{d_{\text{h}}} \quad (1)$$

$$\text{Nu} = \max(\text{Nu}_{\text{lam}}, \text{Nu}_{\text{turb}}) \quad (2)$$

$$\text{Nu}_{\text{lam}} = 3.66 \quad (3)$$

$$\text{Nu}_{\text{turb}} = \frac{\left(\frac{f_{\text{D}}}{8}\right) \cdot (\text{Re} - 1000) \cdot \text{Pr}}{1 + 12.7 \cdot \sqrt{\frac{f_{\text{D}}}{8}} \cdot \left(\text{Pr}^{2/3} - 1\right)} \quad (4)$$

Where k is the thermal conductivity of water and d_h denotes the pipe hydraulic diameter. The Nusselt number is evaluated using standard correlations depending on the local flow regime. If the flow is laminar and fully developed flow (constant wall temperature), equation (3) is used. While for transitional/turbulent regime, Gnielinski correlation (4) is employed for improved accuracy. Therein, the friction factor f_D is calculated following Churchill model for drawn tubing with a surface roughness of 0.00015 mm.

All fluid properties (ρ, μ, k,c_p, Prandtl number) are evaluated at the local bulk temperature. These correlations are implemented pointwise along the pipe network so that h_{int} varies with local Reynolds number and temperature, ensuring consistent treatment of conjugate heat transfer between HTF and the surrounding storage medium.

To reduce computational complexity, a purely seasonal operation profile is adopted. This means that 3 months of charging are followed by 3 months of storage phase, then 3 months of discharging and eventually 3 months of idle phase. During the charging phase, hot water is injected at a temperature of 80°C, while 15°C is the temperature for the injected water during discharging. The injection flow rate corresponds to 0.5 l/s for each entire heat exchange level. Moreover, the loops in H2 and H3 have equivalent flowrate. The outlet pressure is atmospheric corresponding to 1.01325 bar. The initial temperature of both WGTES and ground is 20°C. Further thermophysical properties of the ground are reported in **Table 3**.

Table 3: *Thermophysical properties of the ground.*

Parameter	Value
Ground thermal conductivity	1.4 W/(m·K)
Ground specific heat capacity	2000 J/(kg·K)
Ground density	2100 kg/m^3

Key performance indicators

In this work, three key performance indicators (KPIs) are defined for the technical evaluation of sTES configurations: energy efficiency, energy capacity efficiency and the thermal-to-hydraulic ratio. Among these, the latter serves as a particularly valuable indicator for optimizing the design of charging and discharging heat exchangers. An increase in this ratio reflects a more efficient heat extraction process, whereas excessive pumping power demand may indicate suboptimal hydraulic design, as higher electricity input is required to overcome the system pressure losses.

Table 4: *List of the key performance indicators used in the work.*

KPI	Expression	
Energy efficiency	$\eta_{\text{I}} = \frac{Q_{\text{dis}}}{Q_{\text{ch}}}$	(5)
Energy capacity efficiency	$\eta_{\text{II}} = 1 - \frac{Q_{\text{loss}}}{Q_{\text{TES}}}$	(6)
Thermal-to-hydraulic ratio	$\gamma = \frac{Q_{\text{dis}}}{W_{\text{pump,dis}}}$	(7)

where Q_{ch} and Q_{dis} denote the charged and discharged heat, respectively; Q_{loss} is the total thermal loss to the surroundings; Q_{TES} is the total energy stored in the sTES and $W_{pump,dis}$ represents the electrical work required for pumping during the discharging phase.

Simulation Results and Discussion

Optimal Heat Exchanger Layout

Three indirect charging/discharging heat exchanger configurations based on the Tichelmann concepts were simulated and are hereafter referred to as H1, H2 and H3. The main thermal and hydraulic results are summarized in **Table 5**.

Table 5: *Summary of results for the heat exchanger configurations.*

	H1	H2	H3
Charged energy (MWh)	171	150	160

Discharged energy (MWh)	74	77	88
Energy efficiency (%)	43	50	55
Thermal losses (MWh)	23	57	68
Discharging pump work (MWh)	62	21	20
Thermal-to-hydraulic ratio	1.2	3.3	4.4

From a thermal perspective, configuration H1 achieved the highest charged energy (171 MWh) but exhibited the lowest efficiency of 43% and the highest electrical demand for pump (62 MWh). The limited surface area (322 m²) resulted in homogeneous heat transfer but with higher local hydraulic losses. Consequently, the thermal-to-hydraulic ratio (γ = 1.2) indicates poor coupling between thermal performance and power consumption.

On a brighter note, configuration H2 offered an improved balance. Despite a lower charged energy (150 MWh), the efficiency increased to 50%, whereas the pump work decreased obviously to 21 MWh yielding a thermal-to-hydraulic ratio of 3.3. The larger surface area (448 m²) enhanced the uniformity of heat exchange.

Configuration H3 delivered the best overall performance, with a discharged energy of 88 MWh, efficiency of 55%, and the highest thermal-to-hydraulic ratio (γ = 4.4). The increased surface area (503 m²) promoted effective heat transfer and stable stratification during operation.

Overall, H3 is identified as the optimal layout, providing the most favorable compromise between thermal efficiency, hydraulic performance, and economic viability. These results confirm that increasing the heat-exchange surface area and improving hydraulic balance can significantly enhance system efficiency while maintaining acceptable cost levels.

Thus, the engineering company responsible for the repurposing works selected the heat exchanger configuration for installation in basin C as demonstrated in Figure 10. This decision enables subsequent data acquisition and facilitates model validation, thereby obtaining further trust in the simulation models.

Figure 10: Installation of charging and discharging heat exchangers in basin C with the configuration H3.

Impact of Insulation Quality

An important aspect in the design of sTES is the selection of thermal insulation and its quality. Therefore, this section intends to understand the role of insulation quality on the WGTES performance considering several insulation candidates for basin C at incampus.

Herein, the top insulation layer was kept constant throughout all investigations with U_{top} = 0.15 W/(m^2·K), while the side and bottom insulation materials were systematically varied to assess their impact on the overall heat recovery of the WGTES. Therefore, the insulation thickness was kept to 6 cm for both sidewalls and bottom. Table 6 reports the list of insulation materials investigated in this work for installation on the WGTES sidewalls and bottom.

Table 6: List of insulation materials for WGTES sidewalls and bottom.

Material	$k_{side} = k_{bot}$ W/(m.K)	U W/(m²·K)
EPS/XPS	0.04	0.65
PUR	0.06	0.97
FGG	0.08	1.29
Sawdust	0.1	1.60
Woodchips	0.12	1.90

Figure 11 presents the influence of insulation quality on the thermal performance of the WGTES system over 5 years under the specified boundary conditions. The results show that higher-quality insulation (represented by the uppermost curves) significantly reduces thermal losses, allowing the WGTES to maintain elevated temperatures over successive operational cycles. This leads to improved thermal-to-hydraulic ratio, as a larger fraction of the stored energy remains available for discharge during demand periods. On the other hand, lower-quality insulation (represented by the lower curves) results in increased thermal losses, reducing the effective WGTES volume that can be useful and thereby negatively affecting the thermal-to-hydraulic performance of the system due to lower

energy capacity efficiency (i.e. lower discharged energy).
The trend over multiple years highlights preheating effect of the surrounding ground. While even lower-quality insulation can perform adequately during the first operational year, the difference in recovered thermal energy becomes more pronounced over subsequent years as the ground preheating phases passes and the ground reach quasi steady-state. This demonstrates that long-term monitoring and analyses are highly sensitive to sTES operation.

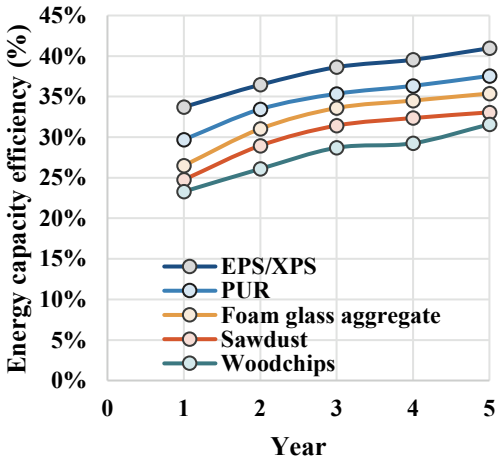

Figure 11: Energy capacity efficiency of incampus basin C with different insulation materials.

Conclusions

This study presented a comprehensive simulation framework for the design and optimization of large-scale seasonal thermal energy storage systems, with application to the incampus water-gravel thermal energy storage. With the aid of COMSOL Multiphysics®, several heat exchanger configurations and insulation materials were evaluated to quantify their impact on thermal performance, hydraulic behavior and overall efficiency. Among the investigated layouts, the configuration of single-sided Tichelmann concept (H3) demonstrated the most favorable balance between thermal efficiency and pump energy demand, leading to its selection for implementation. Sensitivity analyses further highlighted the crucial influence of insulation properties on thermal losses. Outcomes showed that the installation of EPS/XPS led to the highest energy capacity efficiency.

References

[1] A. Dahash, F. Ochs, M. Bianchi Janetti and W. Streicher, "Advances in seasonal thermal energy storage for solar district heating applications: A critical review on large-scale hot-water tank and pit thermal energy storage systems," *Applied Energy,* vol. 239, pp. 296-315, 2019.

[2] C. Bott, I. Dressel and P. Bayer, "State-of-technology review of water-based closed seasonal thermal energy storage systems," *Renewable and Sustainable Energy Reviews,* vol. 113, 2019.

[3] H. Lund, P. A. Østergaard, M. Chang, S. Werner, S. Svendsen, P. Sorknæs, J. Eric Thorsen, F. Hvelplund, B. O. G. Mortensen, B. Vad Mathiesen, C. Bojesen, N. Duic, X. Zhang and B. Möller, "The status of 4th generation district heating: Research and results," *Energy,* vol. 164, pp. 147-159, 2018.

[4] S. Müller, C. Bott, D. Schmitt, M. Faigl, K. Göttl, R. Strobel, P. Bayer and T. Schrag, "Implementation of an expanding thermal source network as a step towards CO2-neutral industry," *Energy,* vol. 330, 2025.

[5] C. Bott, M. Ehrenwirth, C. Trinkl and P. Bayer, "Component-based modeling of ground-coupled seasonal thermal energy storages," *Applied Thermal Engineering,* vol. 214, 2022.

[6] A. Dahash, F. Ochs, A. Tosatto and W. Streicher, "Toward Efficient Numerical Modeling and Analysis of Large-Scale Thermal Energy Storage for Renewable District Heating Systems," *Applied Energy,* vol. 279, 2020.

[7] A. Dahash, F. Ochs, G. Giuliani and A. Tosatto, "Understanding the interaction between groundwater and large-scale underground hot-water tanks and pits," *Sustainable Cities and Society,* 2021.

[8] K. Masera, H. Tannous, V. Stojceska and S. Tassou, "An investigation of the recent advances of the integration of solar thermal energy systems to the dairy processes," *Renewable and Sustainable Energy Reviews,* vol. 172, 2023.

Acknowledgements

The present study is financially supported by the EU Horizon Europe project INTERSTORES (project No. 101136100).Views and opinions expressed are however those of the author(s) only and do not necessarily reflect those of the European Union or Research Executive Agency. Neither the European Union nor the granting authority can be held responsible for them.